Optics Communications 502 (2022) 127340

Contents lists available at ScienceDirect

Optics Communications

journal homepage: www.elsevier.com/locate/optcom

Optimal design of multilayer diffractive optical element in wide angle of incidence

Bo Zhang [a], Keyan Dong [a,*], Mingxu Piao [a], Jianing Wang [b], Ru Jia [c], Huilin Jiang [a]

[a] School of Opto-Electronic Engineering, Changchun University of Science and Technology, Changchun 130022, China
[b] Changchun Institute of Optics, Fine Mechanics and Physics, Chinese Academy of Sciences, Changchun, 130033, China
[c] Institute of Spacecraft System Engineering, Beijing, 100086, China

ARTICLE INFO

Keywords:
Optical system design
Diffractive optics design
Diffraction efficiency
Wide angle of incidence

ABSTRACT

We propose a method for designing the multilayer diffractive optical elements (MLDOEs) to improve the polychromatic integral diffraction efficiency (PIDE) in wide angle of incidence. By comparing and analyzing the characteristic angle weighted PIDE (CAW-PIDE) in the whole angles of incidence, the optimal microstructure height combination of the MLDOE can be obtained. The optimization process and simulation examples for the single-band and multi-band MLDOE are given. Compared to the conventional method, the PIDE is obviously improved in wide angle of incidence by our method. This optimization method can be applied to different working wavebands, and the image quality of the hybrid optical system with the MLDOE can be improved in wide angle of incidence.

1. Introduction

Current imaging instruments require broadband or multi-band lenses to meet the increasing demand for target detection capabilities. As the spectral range increases, it becomes more difficult to achieve high image quality, due to the limitation of optical materials that can be used to achieve achromatic aberration. Diffractive optical elements (DOE) are widely used in various optical systems due to their special negative dispersion characteristics. Therefore, it is a effective way to correct chromatic aberrations by using DOE in broadband or multi-band imaging systems. In addition, the hybrid diffractive–refractive optical system has the advantages of simplified optical structure, miniaturized weight and volume [1–4].

The polychromatic integral diffraction efficiency (PIDE) is the key parameter in determining the working waveband for the DOEs. Multilayer diffractive optical elements (MLDOEs) made of different dispersive materials can achieve high PIDE in broadband or multi-band [5,6]. In Refs. [7–11], the design method of the imaging MLDOE is discussed, but the microstructure height is obtained without considering the incident angle. Compared with the normal incidence, the oblique incidence is the general working situation for imaging MLDOE. In Refs. [12–14], the effects of incident angle on the diffraction efficiency under different conditions are studied, but the method to improve the diffraction efficiency is not discussed in oblique incident situation. In Refs. [15,16], the diffraction efficiency of MLDOEs is improved through the optimized selection of the substrate materials, such as nanocomposite material. However, some of the substrate materials are special, or the limited types of optional multi-band substrate materials, the above method cannot solve the influence of the incident angle on the diffraction efficiency of the MLDOEs.

This paper proposes an optimal design method of MLDOE considering the influence of incident angle. According to the comparison of the characteristic angle weighted PIDEs (CAW-PIDE) at different incident angles, the optimal microstructure heights can be obtained. Compared with the conventional design method of the MLDOE, the PIDE can be improved in wide angle of incidence. This is a general method that can be applied to different wavebands (single-band and multi-band) and different types of MLDOE (double-layer DOE and three-layer DOE).

2. Microstructure heights design method of MLDOEs considering incident angle

The current theories used to describe the optical characteristics of DOEs generally include scalar diffraction theory (SDT) and vector diffraction theory (VDT). When the microstructure period size of the DOE is larger than 14 times the wavelength of the incident light, the SDT can be used to analyze and design the DOE, and accurate results can be obtained [17,18]. Compared with the VDT, the SDT has the advantages of clear theory and simple calculation for designing and analyzing DOEs. The microstructure period width of the MLDOE studied in this paper is generally much larger than the working wavelength in imaging system [19,20], so the accuracy design results can be obtained

* Corresponding author.
E-mail addresses: zhangboyiran@163.com (B. Zhang), dongkeyan@cust.edu.cn (K. Dong).

https://doi.org/10.1016/j.optcom.2021.127340
Received 1 June 2021; Received in revised form 27 July 2021; Accepted 2 August 2021
Available online 5 August 2021

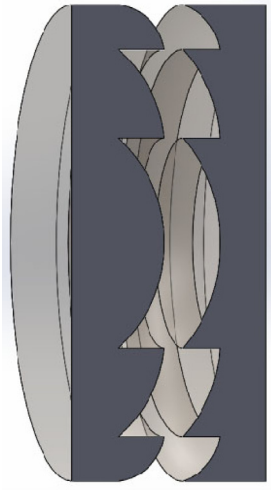

Fig. 1. The structure of the multi-band MLDOE.

by the SDT. The expression of diffraction efficiency for the MLDOE can be written as

$$\eta_m(\lambda,\theta) = \mathrm{sinc}^2\left[m-\phi(\lambda,\theta)\right], \tag{1}$$

where $\mathrm{sinc}(x) = \sin(\pi x)/(\pi x)$, m is the diffraction order. $\phi(\lambda,\theta)$ is the phase retardation of the MLDOE with consideration of incident angle at given period structure, which can be written as

$$\phi(\lambda,\theta) = \frac{\sum_{k=1}^{N}(-1)^{k+1}\left[H_k\left(\sqrt{n_{ki}^2(\lambda)-n_{1i}^2(\lambda)\sin^2\theta}-\sqrt{n_{kt}^2(\lambda)-n_{1i}^2(\lambda)\sin^2\theta}\right)\right]}{\lambda}, \tag{2}$$

where θ is the incident angle of the MLDOE, H_k is the microstructure height of the kth layer, $n_{ki}(\lambda)$ and $n_{kt}(\lambda)$ are the refractive indices of the incident and transmit medium of the kth layer, respectively. N is the total number of layers of the MLDOE. The typical structures of the MLDOE is the double-layer DOE or the three-layer DOE. The multi-layer diffractive optical element in the infrared band is a double-layer DOE, as shown in Fig. 1.

No matter which kind of the MLDOE, there are two microstructure heights need to be designed, so N is usually 2. In order to achieve 100% diffraction efficiency in Eq. (1), both $\phi(\lambda,\theta)$ and m are equal to 1. The microstructure heights of the MLDOE can be expressed as follows in our previous study [15]

$$\begin{cases} H_1 = \dfrac{m\lambda_2 A(\lambda_1) - m\lambda_1 A(\lambda_2)}{B(\lambda_2)A(\lambda_1) - B(\lambda_1)A(\lambda_2)} \\ H_2 = \dfrac{m\lambda_1 B(\lambda_2) - m\lambda_2 A(\lambda_1)}{B(\lambda_2)A(\lambda_1) - B(\lambda_1)A(\lambda_2)} \end{cases}, \tag{3}$$

where

$$\begin{cases} A(\lambda) = \sqrt{n_{2t}^2(\lambda)-n_{1i}^2(\lambda)\sin^2\theta} - \sqrt{n_{2i}^2-n_{1i}^2(\lambda)\sin^2\theta} \\ B(\lambda) = \sqrt{n_{1i}^2(\lambda)-n_{1i}^2(\lambda)\sin^2\theta} - \sqrt{n_{1t}^2-n_{1i}^2(\lambda)\sin^2\theta} \end{cases}, \tag{4}$$

where λ_1 and λ_2 are two design wavelengths. If the MLDOE is used for the dual-band system, λ_1 is selected in the first waveband, and λ_2 is selected in the second waveband. In Refs. [21,22], the actual optical transfer function (OTF) of hybrid optical system can be approximated as the product between the PIDE for DOEs and the theoretical OTF. Therefore, improvement of the PIDE over the entire range of incident angles will be the key to the design of the MLDOE. According to Eqs. (1) and (2), the PIDE of each single waveband for the MLDOE can be written as

$$\begin{cases} \overline{\eta}_m^{B1}(\lambda,\theta) = \dfrac{1}{\lambda_{1\max}-\lambda_{1\min}}\displaystyle\int_{\lambda_{1\min}}^{\lambda_{1\max}} \mathrm{sinc}^2\left[m-\phi(\lambda,\theta)\right]\mathrm{d}\lambda \\ \quad\vdots \qquad\qquad \vdots \\ \overline{\eta}_m^{Bi}(\lambda,\theta) = \dfrac{1}{\lambda_{i\max}-\lambda_{i\min}}\displaystyle\int_{\lambda_{i\min}}^{\lambda_{i\max}} \mathrm{sinc}^2[m-\phi(\lambda,\theta)]d\lambda \\ \quad\vdots \qquad\qquad \vdots \\ \overline{\eta}_m^{BS}(\lambda,\theta) = \dfrac{1}{\lambda_{S\max}-\lambda_{S\min}}\displaystyle\int_{\lambda_{S\min}}^{\lambda_{S\max}} \mathrm{sinc}^2[m-\phi(\lambda,\theta)]d\lambda \end{cases}, \tag{5}$$

where $\overline{\eta}_m^{Bi}$ is the PIDE for the ith waveband. $\lambda_{i\min}$ and $\lambda_{i\max}$ are the minimum and maximum wavelengths for the ith waveband. S is total number of wavebands. The comprehensive PIDE $\overline{\eta}_m^{C}(\lambda,\theta)$ for all wavebands can be written as

$$\overline{\eta}_m^{C}(\lambda,\theta) = \sum_{i=1}^{S} W_i \cdot \frac{1}{\lambda_{i\max}-\lambda_{i\min}}\int_{\lambda_{i\min}}^{\lambda_{i\max}} \mathrm{sinc}^2[m-\phi(\lambda,\theta)]d\lambda, \tag{6}$$

where W_i is the weight of the PIDE for the ith waveband, and the sum of all weights is 1. When the incident angle θ is one of 0° to $\theta_{\max}$, the microstructure heights at different design wavelength combinations can be calculated by Eqs. (3) and (4), and further, the comprehensive PIDE $\overline{\eta}_m^{C}(\lambda,\theta)$ can also be obtained by Eqs. (5) and (6). If the design wavelength combination is different, the microstructure heights and comprehensive PIDE are also different. Therefore, it is possible to find the maximum one among the calculated comprehensive PIDEs to determine the optimal microstructure height combination at the incident angle θ. Based on the obtained optimal microstructure height combination, the comprehensive PIDE values at some characteristic angles can also be calculated, and these calculated values are weighted and summed to obtain the characteristic angle weighted PIDE (CAW-PIDE), which can be expressed as

$$\begin{aligned} \overline{\eta}_m^{CAW}(\lambda) = {} & W_{CAW-1}\times\overline{\eta}_m^{C\_0}(\lambda) + \cdots + W_{CAW-i}\times\overline{\eta}_m^{C\_\frac{\theta_{\max}}{2}}(\lambda) + \cdots \\ & + W_{CAW-j}\times\overline{\eta}_m^{C\_\theta_{\max}}(\lambda), \end{aligned} \tag{7}$$

where W_{CAW-1}, W_{CAW-i} and W_{CAW-j} are the weight factors of the PIDE for different characteristic angles. It should be noted that the number of characteristic angles is selected according to the practical application, not as expressed in Eq. (7). The sum of above weight factors is also 1. For a certain incident angle θ, the unique optimal microstructure height combination can be obtained, and further, the unique CAW-PIDE $\overline{\eta}_m^{CAW}(\lambda)$ can be calculated by given weight factors. When the incident angle θ changes to $\theta+\Delta\theta$, other optimal microstructure height combination and CAW-PIDE $\overline{\eta}_m^{CAW}(\lambda)$ can be obtained. If the CAW-PIDE $\overline{\eta}_m^{CAW}(\lambda)$ for incident angle θ is larger than the CAW-PIDE $\overline{\eta}_m^{CAW}(\lambda)$ for incident angle $\theta+\Delta\theta$, it indicates that the microstructure heights corresponding to θ is more suitable for the wide angle of incidence. Repeating above process, the various CAW-PIDE $\overline{\eta}_m^{CAW}(\lambda)$ can be obtained at different incident angles. The goal is to find the maximum CAW-PIDE $\overline{\eta}_m^{CAW}(\lambda)$, and the corresponding microstructure height combination is the final result. The flow diagram of the optimization process is shown in Fig. 2.

3. Examples and analysis

In order to illustrate the universality of the design method of MLDOE in this paper, the single-band MLDOE and the dual-band MLDOE are analyzed as follows.

3.1. Single-band MLDOEs

For the single-band, the double-layer MLDOE which made of poly (methyl methacrylate) (PMMA) and polycarbonate (PC) [23] is analyzed in the visible waveband (0.4–0.7 μm), and the incident angle

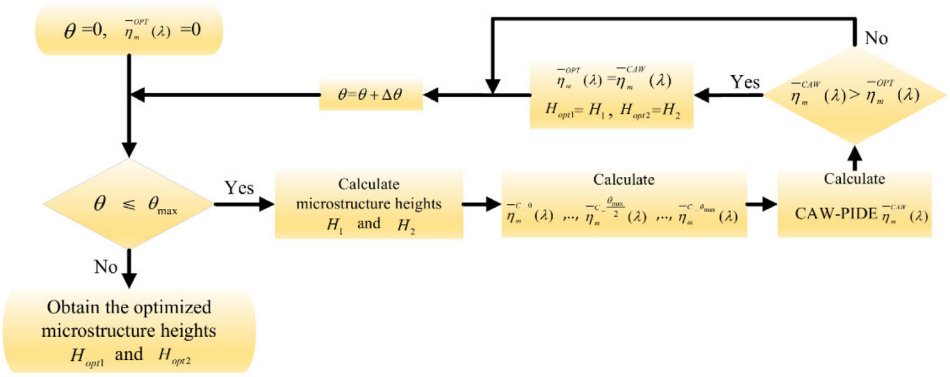

Fig. 2. The flow diagram of the optimization method of MLDOE.

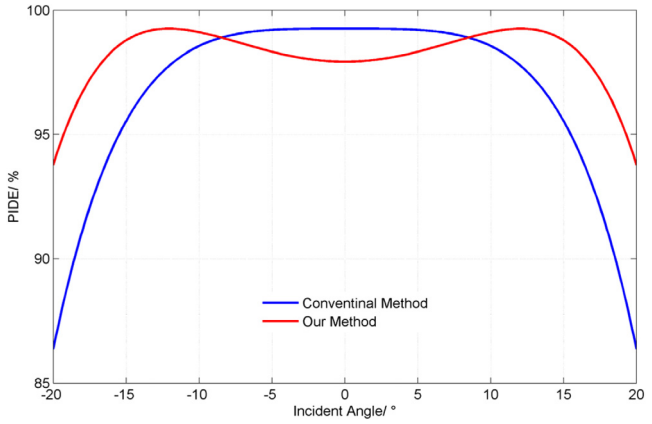

Fig. 3. PIDE versus Incident Angle for Different Design Methods of MLDOE.

Table 1
Comparison of parameters corresponding to different design method of single-band MLDOE.

Parameters	Conventional design method	Optimized design method
H_1 (μm)	16.5526	16.2221
H_2 (μm)	−12.8892	−12.6725
PIDE at 0° (%)	99.2514	97.9284
PIDE at 20° (%)	86.3675	93.7716

range is $-20^o \le \theta \le 20^o$. Since there is only one working waveband, the Eqs. (5) and (6) are simplified to the same expression, and $\lambda_{1\,\min}$ and $\lambda_{1\,\max}$ are 0.4 μm and 0.7 μm, respectively. The incident angles 0°, 10° and 20° are selected as the characteristic angles, and corresponding weight factors are $W_{CAW-1} = 0.45$, $W_{CAW-2} = 0.3$ and $W_{CAW-3} = 0.25$. According to the above optimization process of the MLDOE, a mass of PIDEs for characteristic angles $\bar{\eta}_m^{C\_0}(\lambda)$, $\bar{\eta}_m^{C\_10}(\lambda)$ and $\bar{\eta}_m^{C\_20}(\lambda)$ are calculated, and then, a mass of CAW-PIDE $\bar{\eta}_m^{CAW}(\lambda)$ are also obtained when the incident angle θ gradually increases from 0° to 20°. By repeatedly comparing the obtained $\bar{\eta}_m^{CAW}(\lambda)$, the maximum one can be finally found, that is $\bar{\eta}_m^{CAW}(\lambda) = 97.24\%$, and the corresponding microstructure heights are the optimal result. The relationship between incident angle and the PIDE is shown in Fig. 3. The PIDE at different incident angles are listed in Table 1.

In Fig. 3, the blue line and red line represent the analysis results of the conventional design method [9–11] and our design method, respectively. Because the influence of the incident angle on the PIDE is not considered in the conventional design method, the PIDE decreased from 99.2514% at 0° to 86.3675% at 20°, and the reduction is 12.8839%, as listed in Table 1. Finally, the imaging quality of the maximum field of view will be seriously affected by the MLDOE. Compared to the blue line, the PIDE is obviously improved when the incident angle is 20°, and the PIDE increases from 86.3675% to 93.7716% (an increase of 7.4041%) in red line. When the incident angle is 0°, the PIDE decreases from 99.2514% to 97.9284% (a reduction of 1.323%). This reduction of the PIDE is almost 1%, and the image quality influence at the axial field is acceptable in practical applications. The relationship among diffraction efficiency, wavelength and incident angle is shown in Fig. 4.

In Fig. 4, the two abscissas represent the wavelength and incident angle, respectively, and the vertical coordinate represents the diffraction efficiency. From Fig. 4, we can see that the most of diffraction efficiency is obviously improved after microstructure heights optimization, especially at the edge of the incident angle range.

3.2. Dual-band MLDOEs

For the dual-band MLDOE, the working wavebands are the mid-wave infrared (MWIR, 3–5 μm) and long-wave infrared (LWIR, 8–12 μm). The substrate materials of dual-band MLDOE are Zinc Sulfide (ZNS) and Zinc Selenide (ZNSE) [24]. The ZNSE is the incident substrate and ZNS is the emergent substrate. The incident angle range is $-10^o \le \theta \le 10^o$. Because the MLDOE is applied to infrared dual-band, λ_1 is selected in the MWIR, and λ_2 is selected in the LWIR in Eq. (3). According to the design wavelengths, the microstructure height combination can be calculated, and the PIDE $\bar{\eta}_m^{B1}$ and $\bar{\eta}_m^{B2}$ for the MWIR and LWIR can also be obtained by Eq. (5). The wavelength $\lambda_{1\,\min}$ is 3 μm, $\lambda_{1\,\max}$ is 5 μm, $\lambda_{2\,\min}$ is 8 μm and $\lambda_{2\,\max}$ is 12 μm. Further, the comprehensive PIDE $\bar{\eta}_m^{C}(\lambda,\theta)$ can be calculated by Eq. (6), and weight $W_1 = 0.7$ for the MWIR and $W_2 = 0.3$ for the LWIR. The incident angles 0°, 5° and 10° are selected as the characteristic angles, and corresponding weight factors are $W_{CAW-1} = 0.4$, $W_{CAW-2} = 0.3$ and $W_{CAW-3} = 0.3$. According to given weight factors and calculated comprehensive PIDEs for characteristic angles, the CAW-PIDE $\bar{\eta}_m^{CAW}(\lambda)$ can be calculated by Eq. (7). When the incident angle θ is increased from 0° to 10°, a mass of $\bar{\eta}_m^{CAW}(\lambda)$ can be calculated, and the maximum one ($\bar{\eta}_m^{CAW}(\lambda) = 96.53\%$) can be found by repeating comparison, as shown in Fig. 2. Finally, the optimal microstructure heights can be obtained for the dual-band MLDOE, as listed in Table 2. The relationship between incident angle and comprehensive PIDE is shown in Fig. 5.

In Fig. 5, the blue line and red line represent the analysis results of the conventional design method and our design method, respectively. Similar to the single-band MLDOE, the comprehensive PIDE is reduced obviously for the blue line when the incident angle increases. By optimizing the microstructure heights, the comprehensive PIDE at 10° is increased from 90.3543% to 93.8805% (an increase of 3.5262%). When the incident angle is 0°, the comprehensive PIDE is decreased from 97.9717% to 97.4522% (a reduction of 0.5195%) for the red

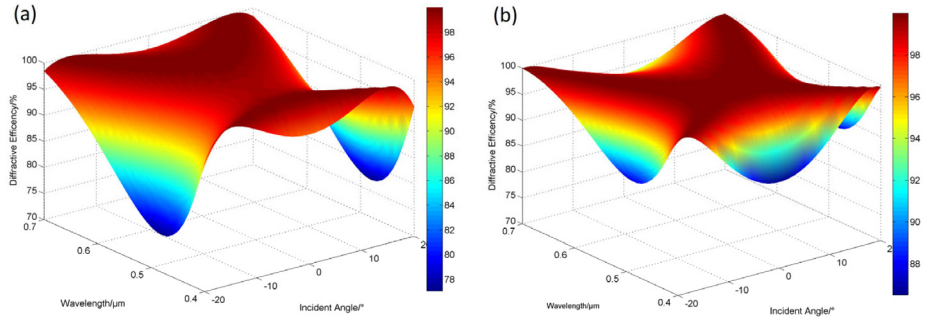

Fig. 4. Diffraction Efficiency versus Wavelength and Incident Angle for MLDOE using Different Design Methods. (a) Conventional Method. (b) Our Method.

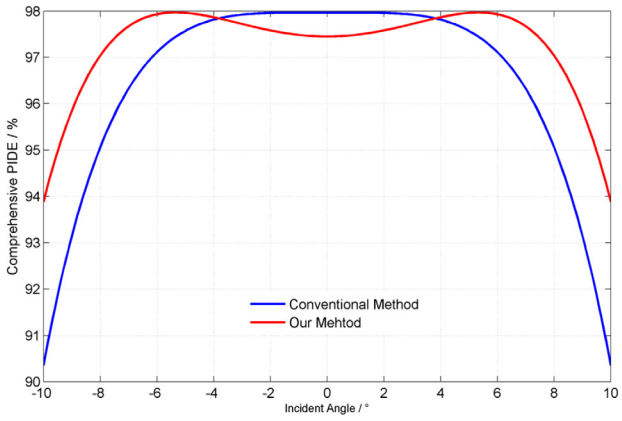

Fig. 5. Comprehensive PIDE versus Incident Angle for Different Design Methods of Dual-band MLDOE.

Table 2
Comparison of parameters corresponding to different design method of multi-band MLDOE.

Parameters	Conventional design method	Optimized design method
H_1 (μm)	187.3395	186.4175
H_2 (μm)	−211.2708	−210.0697
$\overline{\eta}_m^C(\lambda,\theta)$ at 0° (%)	97.9717	97.4522
$\overline{\eta}_m^C(\lambda,\theta)$ at 10° (%)	90.3543	93.8805
MWIR PIDE at 0° (%)	97.8190	97.0733
MWIR PIDE at 10° (%)	87.5405	92.3218
LWIR PIDE at 0° (%)	98.3282	98.3363
LWIR PIDE at 10° (%)	96.9197	97.5174

line. Because the comprehensive PIDE is changed for different design methods, the PIDE for MWIR and LWIR are also changed, as shown in Fig. 6. The PIDE for each waveband are listed in Table 2.

In the MWIR, the PIDE increases from 87.5405% to 92.3218% (an increase of 4.7813%) after optimizing microstructure heights when the incident angle is 10°. Compared with conventional method, the image quality at maximum field of view is improved after microstructure height optimization. When the incident angle is 0°, the PIDE decreases from 97.8190% to 97.0733% (a reduction of 0.7457%) for the red line. Because of the PIDE reduction is less than 1%, the decline of image quality at axial field can be ignored. In the LWIR, the PIDE increases from 96.9197% to 97.5174% (an increase of 0.5977%) when the incident angle is 10°. When the incident angle is 0°, the PIDE increases from 98.3282% to 98.3363% (an increase of 0.0081%) for the red line. Different from the MWIR, the PIDE of the LWIR is improved for entire incident angle range, so the image quality of the LWIR can be improved at all field of view after microstructure height optimization. The relationship among diffraction efficiency, wavelength and incident angle is shown in Fig. 7.

From Fig. 7, the diffraction efficiency is obviously improved at the edge of the incident angle range after microstructure height optimization in MWIR. At the same time, the diffraction efficiency is improved throughout the incident range in LWIR.

4. Conclusions

In conclusion, we put forward an optimal design method of the imaging MLDOE to improve the PIDE in wide angle of incidence for the first time. The relationship between the PIDE and incident angle is theoretically analyzed, and the characteristic angle weighted PIDE (CAW-PIDE) is presented to determine the optimal microstructure height combination. The detailed optimization process of the MLDOE is given, and the simulation examples for the visible broadband MLDOE and infrared dual-band MLDOE are analyzed. Compared to the conventional methods, the PIDE is obviously improved throughout the incident range. The presented results are of great significance for practical

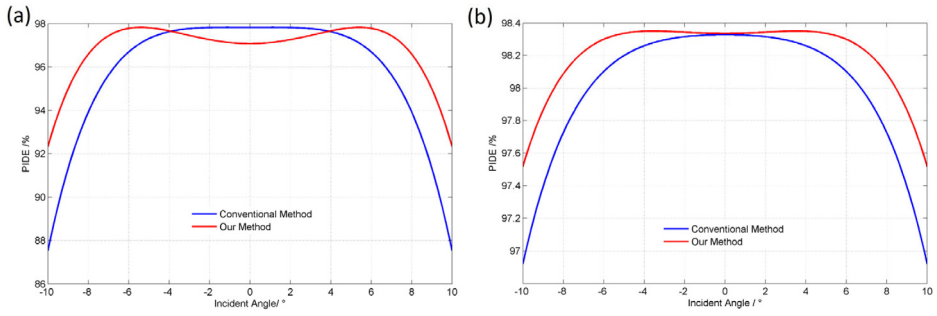

Fig. 6. PIDE versus Incident Angle for Different Design Methods of Dual-band MLDOE. (a) MWIR. (b) LWIR.

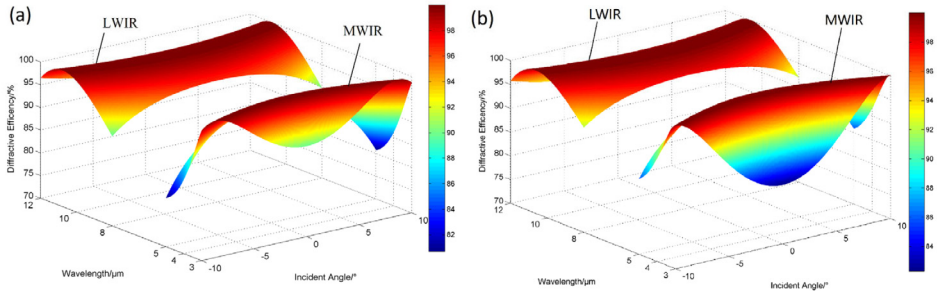

Fig. 7. Diffraction Efficiency versus Wavelength and Incident Angle for Dual-band MLDOE using Different Design Methods. (a) Conventional Method. (b) Our Method.

design of the hybrid optical imaging system with the different kinds of MLDOEs in wide angle of incidence.

Declaration of competing interest

The authors declare that they have no known competing financial interests or personal relationships that could have appeared to influence the work reported in this paper.

Funding

This work was supported by the Excellent Youth Foundation of Jilin Province Scientific Committee, China (20190103134JH); The National Natural Science Foundation of China Youth Fund (62005268).

References

[1] H. Zhang, H. Liu, A. Lizana, W. Xu, J. Caompos, Z. Lu, Methods for the performance enhancement and the error characterization of large diameter ground-based diffractive telescopes, Opt. Express 25 (2017) 26662–26677.
[2] Y. Hu, Q. Cui, L. Zhao, M. Piao, PSF model for diffractive optical elements with improved imaging performance in dual-waveband infrared systems, Opt. Express 26 (2018) 26845–26857.
[3] Y. Bian, Y. Liu, L. Jiang, Design of double-zone aspheric diffractive intraocular lens with extended depth of focus, Chin. Opt. Lett. 16 (2018) 093301.
[4] G.I. Greisukh, E.G. Ezhov, Z.A. Sidyakina, S.A. Stepanov, Design of plastic diffractive-refractive compact zoom lenses for visible-near-IR spectrum, Appl. Opt. 52 (2013) 5843–5850.
[5] Y.G. Soskind, Diffractive optics technologies in infrared systems, Proc. SPIE 9451 (2015) 94511T.
[6] A. Wood, M.L. Lee, S. Cassette, Infrared hybrid optics with high broadband efficiency, Proc. SPIE 5874 (2005) 58740G.
[7] Y. Aredli, S. Ozeri, N. Eisenberg, Design of a diffractive optical element for wide spectral bandwidth, Opt. Lett. 23 (1998) 823–824.
[8] T. Gühne, J. Barth, Strategy for design of achromatic diffractive optical elements with minimized etch depths, Appl. Opt. 52 (2013) 8419–8423.
[9] X. Dun, W. Jin, X. Wang, Material selection and corresponding optimal surface relief height for multilayer diffractive optical elements, Opt. Eng. 54 (2015) 115105.
[10] C. Xue, Q. Cui, Design of multilayer diffractive optical elements with polychromatic integral diffraction efficiency, Opt. Lett. 35 (2010) 986–988.
[11] C. Xue, Q. Cui, T. Liu, L. Yang, B. Fei, Optimal design of a multilayer diffractive optical element for dual wavebands, Opt. Lett. 35 (2010) 4157–4159.
[12] L. Yang, C. Liu, S. Li, Optimal design of depth-scaling error for multilayer diffractive optical elements with oblique incidence, Appl. Opt. 56 (2017) 4532–4536.
[13] S. Mao, Q. Cui, M. Piao, L. Zhao, High diffraction efficiency of three-layer diffractive optics designed for wide temperature range and large incident angle, Appl. Opt. 55 (2016) 3549–3554.
[14] H. Yang, C. Xue, C. Li, J. Wang, R. Zhang, Diffraction efficiency sensitivity to oblique incident angle for multilayer diffractive optical elements, Appl. Opt. 55 (2016) 7126–7133.
[15] B. Zhang, Q. Cui, M. Piao, Y. Hu, Design of dual-band infrared zoom lens with multilayer diffractive optical elements, Appl. Opt. 58 (2019) 2058–2067.
[16] D. Werdehausen, S. Burger, I. Staude, T. Pertsch, M. Decker, Dispersion-engineered nanocomposites enable achromatic diffractive optical elements, Optica 6 (8) (2019) 1031–1038.
[17] S. Peterhansel, C. Pruss, W. Osten, Limits of diffractometric reconstruction of line gratings when using scalar diffraction theory, Opt. Lett. 39 (13) (2014) 3764–3766.
[18] G.J. Swanson, Binary Optics Technology: Theoretical Limits on the Diffraction Efficiency of Multilevel Diffractive Optical Elements, MIT Lincoln Laboratory Technical Report 914, 1991.
[19] Andrew Wood, Mane-Si Laure Lee, Simone Cassette, Infrared hybrid optics with high broadband efficiency, Proc. SPIE 5874 (2005) 58740G.
[20] Jun-ichi Kudo, Hideo Wada, Toshihiro Okamura, Masako Kobayashi, Kunihiro Tanikawa, Diffractive lens in 8- to 10-μm forward-looking infrared system, Opt. Eng. 41 (8) (2002) 1787–1791.
[21] D.A. Buralli, G.M. Morris, Effects of diffraction efficiency on the modulation transfer function of diffractive lenses, Appl. Opt. 31 (1992) 4389–4396.
[22] C. Bigwood, New infrared optical systems using diffractive optics, Proc. SPIE 4767 (2002) 1–12.
[23] M. Bass, G. Li, E.V. Stryland, Handbook of Optics, vol. IV, McGraw-Hill, 2010.
[24] M.J. Riedl, Optical Design Fundamentals for Infrared Systems, second ed., SPIE, 2001.